Flexible Density-based Multipath Component Clustering Utilizing Ground Truth Pose

Whiton, Russ; Chen, Junshi; Tufvesson, Fredrik

Published in:
2023 98th Vehicular Technology Conference (VTC2023-Fall)

2023

Document Version:
Early version, also known as pre-print

Flexible Density-based Multipath Component Clustering Utilizing Ground Truth Pose

Russ Whiton*‡, Junshi Chen†‡, Fredrik Tufvesson‡
*Volvo Car Corporation, SE-405 31 Gothenburg, Sweden
†Terranet AB, Lund, Sweden
‡Dept. of Electrical and Information Technology, Lund University, Lund, Sweden
Email: {russell.whiton, junshi.chen, fredrik.tufvesson}@eit.lth.se

***Abstract*—Accurate statistical characterization of electromagnetic propagation is necessary for the design and deployment of radio systems. State-of-the-art channel models such as the Enhanced COST 2100 Channel Model utilize the concept of clusters of multipath components, and characterize channels by their inter- and intra-cluster statistics. Automatic clustering algorithms have been proposed in literature, but the subjective nature of the problem precludes any from being deemed objectively correct. In this paper, a new algorithm is proposed, based on density-reachability and ground truth receiver pose, with the explicit focus of extracting clusters for the purpose of channel characterization. Measurements of downlink signals from a commercial LTE base station by a passenger vehicle driving in an urban environment with a massive antenna array on the roof are used to evaluate the repeatability and intuitiveness of the proposed clustering algorithm.**

***Index Terms*—Automatic clustering algorithm, Channel Modeling, Massive MIMO, Software defined radio.**

I. Introduction

Radio systems have made enormous leaps in capabilities in recent decades, and are intricately woven into the fabric of modern industrial society. The International Telecommunication Union (ITU) suggests that increased data traffic volume, diversified service requirements, higher demands on Quality-of-Service (QoS) and cost pressure will necessitate innovative solutions for future development [1]. Maximizing spectral efficiency can be antithetical to achieving Ultrareliable and Low-Latency Communication (URLLC), for example [2], and all parameters of future systems require close scrutiny to meet the ITU vision for this evolution.

One fundamental building block for designing radio systems to meet these diverse requirements is a deep understanding of electromagnetic wave propagation. Physical models for wave propagation have been developed explicitly for this purpose, and typically models are employed in which the channel is characterized as a number of discrete Multipath Components (MPCs) originating at the transmitter and impinging upon the receiver [3]. Sometimes the concept of *dense multipath* [4] is also included in the model, in which one or more exponential functions in the time domain are also jointly considered. The modeling of these MPCs is typically done either with site-specific channel models (including ray models) where the complete wave trajectories are determined analytically, or alternatively the parameters of MPCs are treated stochastically [5]. Stochastic modeling has enjoyed widespread attention, especially Geometry-based Stochastic Channel Models (GSCMs), because GSCMs can be generalized broadly and are of utility for many aspects of system design and verification. Since the advent of Third Generation (3G) cellular systems, GSCMs have evolved from an MPC-based understanding of propagation to a *cluster*-based understanding, in which MPCs sharing similar properties are grouped together [6].

However, the cluster-based understanding of radio channels necessarily entails ambiguity about the definition of a cluster, and it would be difficult or impossible to define a single objective metric for this purpose. Early work in MPC clustering relied on visual analysis of the delay-domain arrival of MPCs, but subsequent work has resulted in numerous proposals for automatic clustering algorithms operating in other domains. The algorithms also differ in their applicability across frequencies and measurement environments, the number of parameters required for tuning, and whether they are intended to work in real-time or in post-processing. There still appears to be a need for an intuitive and flexible algorithm for MPC clustering which is scalable to large data sets.

In this paper, a novel automatic clustering algorithm is proposed for rapid and repeatable clustering of large channel measurement data sets for propagation modeling, utilizing precise estimates of receiver position and orientation. The proposed model uses DBSCAN [7] in *odometry space* (defined in Sec. II), and is evaluated on test data received by a passenger vehicle-mounted measurement system operating in an urban environment, receiving 2.66 GHz downlink signals from a commercial Long-Term Evolution (LTE) base station paired with a high-end ground truth positioning system. The clustering algorithm has the following salient features:

- Simultaneous consideration of the entire measurement series when performing clustering, eliminating any need for inner/outer filters for cluster birth/death processes operating across a time series.
- Cluster definitions directly influenced by physical movement of the receiver, so-called Visibility Regions (VRs).
- Applicability across frequencies and geometries.
- Consideration of second-order and higher reflections.
- Simple parameter tuning with intuitive physical interpretation, and quick map-based visualization of results.

The paper is organized as follows: Section II provides background on clustering algorithms and describes the proposed algorithm; Section III discusses the measurement system and data collection campaign; Section IV provides the results of the measurements; and finally Section V offers conclusions and suggestions for future work.

Notes on mathematical representation:

- Vectors are indicated in lower-case bold font $\boldsymbol{x}$ or $\boldsymbol{\omega}$
- $\|\boldsymbol{x}\|$ indicates the L2-norm of vector $\boldsymbol{x}$
- $\{x_{a,b}\}$ is the set of $x_{a,b}$ for all valid combinations of a and b

II. Multipath Component Clustering

A. Waves and Clusters

In the field of propagation modeling, the double-directional channel response is typically modeled as the superposition of L waves (planar or spherical) originating at the transmitter and arriving at the receiver. The waves are parameterized by their delays τ_l, the angles-of-departure Ω_l^{TX} and arrival Ω_l^{RX} (which can be further subdivided into azimuthal angles-of-arrival/departure ϕ_l^{RX} and ϕ_l^{TX}, and elevation-of-arrival/departure θ_l^{RX} and θ_l^{TX}), the complex-valued path loss α_l and Doppler shift[1] ψ_l:

$$h(t,\tau,\Omega^{TX},\Omega^{RX},\psi)=\sum_{l=1}^{L}h(t,\alpha_l,\tau_l,\Omega_l^{TX},\Omega_l^{RX},\psi_l). \quad (1)$$

In a seminal work on electromagnetic propagation modeling, the authors observed that MPCs tend to arrive in clusters of similar delay and uniformly distributed random phase [8], use of this observation allows for more precise modeling of the channel rather than treating the arrival of individual MPCs as a Poisson process. Clusters of MPCs with similar propagation parameters (including delays, angles and Doppler frequencies) are distinguishable from other clusters with different propagation parameters because the objects that the electromagnetic waves interact with typically give rise to several paths simultaneously with similar geometries [9]. Understanding the nature of clusters continues to be an active area of research, with the Enhanced COST 2100 channel model setting a new state-of-the-art in sophistication [5] and reformulating the channel in terms of C clusters, each with L_c MPCs. The channel has an overall path-loss G, and each cluster has its own visibility gain V_c, shadow fading S_c and cluster attenuation G_c. This cluster-based formulation of the channel response is expressed as a double summation over clusters and the MPCs within each cluster:

$$h(t,\tau,\Omega^{TX},\Omega^{RX},\psi)= \frac{1}{G}\sum_{c=1}^{C}V_c\sqrt{\frac{S_c}{G_c}}\sum_{l=1}^{L_c}h(t,\alpha_{l,c},\tau_{l,c},\Omega_{l,c}^{TX},\Omega_{l,c}^{RX},\psi_{l,c}). \quad (2)$$

[1]Polarization is omitted in this work, as in [4], for brevity, but could also be considered for clustering if desired.

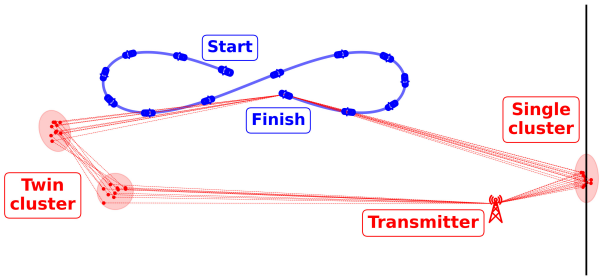

Fig. 1: An example clustering scenario. A vehicle drives a short trajectory and receives signals from two clusters, one of which has a single reflection and another stemming from a double reflection. Rays are illustrated for the last snapshot.

Clusters can be classified as local clusters, single clusters, or twin clusters depending on the geometry. Fig. 1 illustrates two clusters for a mobile receiver traversing a short figure-eight trajectory. One single cluster and one twin cluster are visible, and the MPCs for the final snapshot of the trajectory are illustrated.

B. Automatic Clustering Algorithms

Pioneering work on MPC clusters identified inter- and intra-cluster parameters in the delay domain through visual inspection of a limited data set [8]. The Random-Cluster Model was presented in [3], which compared hierarchical tree clustering and KPowermeans. Kernel-Power-Density was suggested in [10], and a modified DBSCAN algorithm was proposed in [11], with the latter mapping clusters to physical points in space on a single-bounce cluster assumption, i.e., no twin clusters are considered. The motivations for all these novel automatic clustering algorithms have emphasized the ambiguity and fallibility of visual clustering, the need for scalability and repeatability, and the value of minimizing user-specified parameters.

Some shortcomings are apparent with the existing clustering algorithms. Visual identification of MPCs in the delay or even angle-delay domain quickly becomes difficult not only with increasing numbers of MPCs and clusters, but also with movement and rotation of the measurement apparatus (for Ω^{RX}) or a mobile transmitter (for Ω^{TX}). This can be partially mitigated through joint clustering and tracking, in which measurements are processed sequentially to keep track of clusters, MPCs and dense multipath [12], but this makes tuning difficult in that it requires cluster birth/death processes with their heuristics for data association. Fig. 2 shows simulated measurement data for the scenario of Fig. 1. Examining the entire measurement series together without regard for the time evolution (left side) results in ambiguity regarding the number of clusters and their shape. Joint clustering and tracking using the time series (right side) should permit effective differentiation in this case. Either a sliding window or filtering is typically used to increase stationarity, but window size also impacts performance. For the purpose of propagation modeling, as opposed to real-time operation, it is desirable to define clusters based on

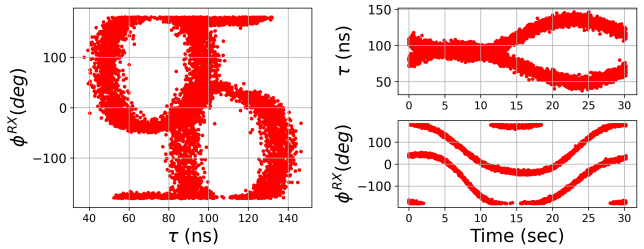

Fig. 2: (Left) Clustering in the Angle-of-Arrival-Delay Domain for the full measurement series in Fig. 1. Drawing a clear boundary between the two clusters in this view is difficult. (Right) Time series view of the same measurements intended for joint clustering and tracking. Cluster identification in the time series of the angular domain is more obvious.

the complete data set simultaneously, rather than sequentially processing the measurements.

In the COST 2100 Channel Model, it is implicit that motion in space (and *not* change in time) causes channel statistics to change, and clusters are understood to correspond with ellipsoids at fixed points in space associated with movement in and out of VRs [9]. In the Random Cluster Model, clusters are treated as "moving" with time (apparent in the time series of Fig. 2). Transmitter or receiver rotation should not impact the view of the cluster[2], but rather physical movement is what impacts visibility.

C. A New MPC Clustering Algorithm

With these limitations in mind, in this subsection a novel MPC clustering algorithm is proposed based on density-reachability using DBSCAN [7]. DBSCAN is a clustering algorithm that elegantly captures arbitrarily-shaped clusters with only two tuning parameters and a distance criterion. The first tuning parameter, ϵ, is a heuristic for deciding "reachability" between two points in one or more dimensions y^p and y^q according to the distance criterion $d(y^p, y^q)$, and the second tuning parameter N_{min} governs the number of reachable points for classification of "core points" around which the clusters are subsequently defined. DBSCAN and its extensions are thoroughly described in other literature, e.g., [13], so the algorithm details are not restated in this paper.

Some of the compelling strengths of DBSCAN are not fully realized with previous application for MPC clustering [11]. The algorithm scales well for large data sets, but channel estimation algorithms rarely estimate more than tens of MPCs for a single snapshot, particularly subspace-based channel estimation methods. An additional unrealized strength of DBSCAN is that the clustering domain can also be formulated in a highly abstract manner, meaning that *a strict interpretation of MPC physical location is unnecessary*. Twin clusters can be captured with higher abstraction, as well as single-bounce clusters or Line-of-Sight (LOS) clusters. In this subsection a method is described in which MPCs are first mapped into *vehicle space*, the coordinate system of the vehicle, then rotated and shifted into a world coordinate system *projected space* (but not their true location, with the exception of the LOS MPCs), and finally receiver movement is added as an arbitrary dimension (a dimension tailored to conform with the concept of VRs) for extension into *odometry space* before clustering is performed with DBSCAN.

The complete 6-dimensional pose of the receiver for snapshot index t is expressed in terms of three-dimensional position, in meters, defined in an East-North-Up (ENU) frame[3] $\boldsymbol{p}_t = [e_t, n_t, u_t]^T$ as well as three-dimensional orientation in terms of yaw, pitch and roll angles in radians $\boldsymbol{\omega}_t = [\gamma_t, \lambda_t, \eta_t]^T$. For each snapshot t, a variable number of MPCs L_t are estimated per Equation (1). The angles-of-arrival and component delays of these individual MPCs $\theta_{l,t}^{RX}$, $\phi_{l,t}^{RX}, \tau_{l,t}$, are first translated from spherical form into vector form and scaled by their total path lengths into *vehicle space*[4] denoted $\boldsymbol{\psi}_{l,t}$:

$$\boldsymbol{\psi}_{l,t} = \begin{bmatrix} \psi_{l,t}^{forw} \\ \psi_{l,t}^{left} \\ \psi_{l,t}^{abov} \end{bmatrix} = \tau_l \begin{bmatrix} sin(\theta_{l,t})cos(\phi_{l,t}) \\ sin(\theta_{l,t})sin(\phi_{l,t}) \\ cos(\theta_{l,t}) \end{bmatrix}. \tag{3}$$

Individual MPCs in vehicle space are subsequently rotated and translated into the ENU frame by using both the orientation $\boldsymbol{\omega}_t$ and position $\boldsymbol{p}_t$ of the receiver at the relevant epoch. These projections are denoted *projection space* and represented by $\boldsymbol{\zeta}_{l,t}$:

$$\boldsymbol{\zeta}_{l,t} = \begin{bmatrix} \zeta_{l,t}^{e} \\ \zeta_{l,t}^{n} \\ \zeta_{l,t}^{u} \end{bmatrix} = \begin{bmatrix} \psi_{l,t}^{forw} \\ \psi_{l,t}^{left} \\ \psi_{l,t}^{abov} \end{bmatrix} \begin{bmatrix} 1 & 0 & 0 \\ 0 & cos(\eta_t) & sin(\eta_t) \\ 0 & -sin(\eta_t) & cos(\eta_t) \end{bmatrix} \begin{bmatrix} cos(\lambda_t) & 0 & -sin(\lambda_t) \\ 0 & 1 & 0 \\ sin(\lambda_t) & 0 & cos(\lambda_t) \end{bmatrix} \begin{bmatrix} cos(\gamma_t) & sin(\gamma_t) & 0 \\ -sin(\gamma_t) & cos(\gamma_t) & 0 \\ 0 & 0 & 1 \end{bmatrix} - \begin{bmatrix} e_t \\ n_t \\ u_t \end{bmatrix}. \tag{4}$$

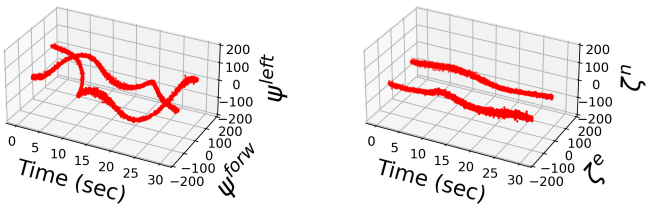

Fig. 3: (Left) Representation of MPCs $\boldsymbol{\psi_l}$ in vehicle space for the scenario in Fig. 1. (Right) Time evolution of MPCs in an external reference frame (projection space) using vehicle pose including $\boldsymbol{p}_t$ and $\boldsymbol{\omega}_t$, which constrains apparent motion of cluster locations.

Vector representations of MPCs for the scenario depicted in Fig. 1 are illustrated in Fig. 3. In the vehicular coordinate system, the evolution of MPCs $\boldsymbol{\psi}_l$ clearly follows the

[2]The antenna radiation patterns will of course impact the complex channel gain.

[3]Position can be expressed equivalently in any arbitrarily defined reference frame.

[4]The vehicular system used is Forward-Left-Above, per the ISO8855 standard.

heading change of the vehicle, and while the two clusters are distinguishable by inspection, the apparent movement in the vehicular frame may appear to be a series of unlikely innovations for a filter tracking the cluster locations. In the ENU frame, cluster movement is smaller in absolute terms.

A physical interpretation of vehicular space for the clusters in Fig. 1 is illustrated in Fig. 4. In the vehicular coordinate system, the clusters appear to wander and joint clustering and tracking would entail using the time series to track the moving cluster center locations and deciding whether to expand or contract the number of clusters. Fig. 5 shows the same scenario in projected space. Depending on the order (LOS, single or twin cluster) and type of the reflector, aggregated MPCs with similar parameters will define either concentrated clouds or arcs as the receiver moves through VRs.

The final step in MPC representation is to append to each MPC the associated odometry value of the measurement apparatus χ_t for extension into odometry space. In this manner, arcs that project to the same location in projection space will be separated when clustering, which improves scalability to large data sets where the projection space might become crowded. This is shown in Fig. 6. When exiting a VR, additional movement will create separation in the odometry dimension. Multiple passes through the same VR, separated by movement outside the VR, will generate new clusters:

$$\chi_t = \int_0^t \left\| \frac{d}{dt}\boldsymbol{p}_t \right\| = \int_0^t \left\| \begin{bmatrix} \frac{\partial}{\partial t} e_t \\ \frac{\partial}{\partial t} n_t \\ \frac{\partial}{\partial t} u_t \end{bmatrix} \right\|. \tag{5}$$

The final representation of each MPC in odometry space consists of the three-dimensional projected points[5] and the associated odometry value, i.e., $\boldsymbol{y}_{l,t} = [\chi_t, \zeta^e_{l,t}, \zeta^n_{l,t}, \zeta^u_{l,t}]^T$. The odometry space version of the MPCs for the twin cluster of Fig. 1 is shown in Fig. 6.

DBSCAN is applied directly to the points in odometry space. For the measurements described in Sec. III, $N_{min} = 15$, $\epsilon = 8$ and the distance criterion is Euclidian distance in odometry space, i.e., $d(\boldsymbol{y}^p, \boldsymbol{y}^q) = \|\boldsymbol{y}^p - \boldsymbol{y}^q\|$. For three-dimensional projections, visualization in odometry space can be accomplished through compression in one position dimension, as Fig. 6 does for the vertical spatial dimension (altitude). More concisely, given the entire set of all odometry space MPCs $\{\boldsymbol{y}_{l,t}\}$ for all T snapshots, DBSCAN assigns a label p to each member of the set:

$$DBSCAN : \{\boldsymbol{y}_{l,t}\} \rightarrow \{\boldsymbol{y}_{l,t,p}\}. \tag{6}$$

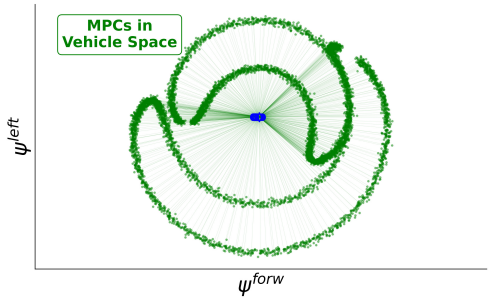

Fig. 4: MPCs from the scenario in Fig. 1 in vehicle space. Vehicle movement results in an apparent movement of the cluster locations.

[5]Projection could be done in a similar fashion using angles-of-departure either as an alternative or simultaneously, but the measurement system described in Sec. III is not fully double-directional.

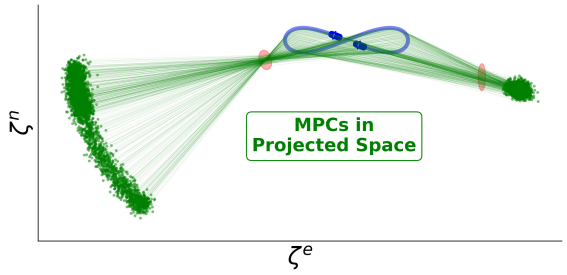

Fig. 5: MPCs from Fig. 1 shown in projection space. Projected MPCs in the external coordinate system do not correspond with the physical locations, except for the LOS path.

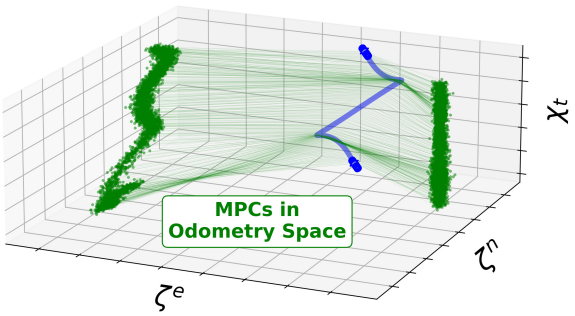

Fig. 6: MPCs from Fig. 1 in odometry space, the domain in which DBSCAN is applied. Overlapping arcs in physical space will not be clustered together if no neighborhood can be established with consideration for the ϵ parameter in physical space, i.e., with sufficient receiver movement.

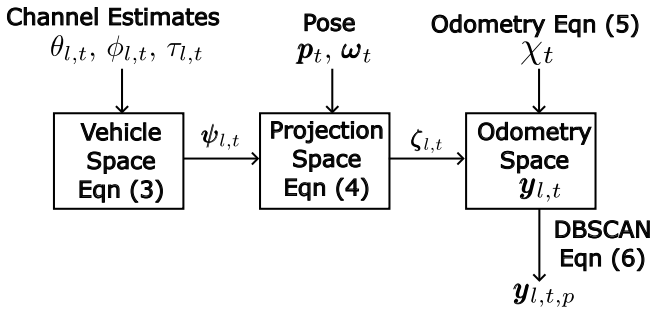

Fig. 7: Flow chart describing the novel clustering algorithm. MPCs are transformed into the odometry space domain before clustering is applied with DBSCAN.

The number of clusters P is not pre-defined, and points classified as noise (not density-reachable from a core point) are assigned a label of -1. The algorithm steps are summarized in Fig. 7.

III. LTE Measurements

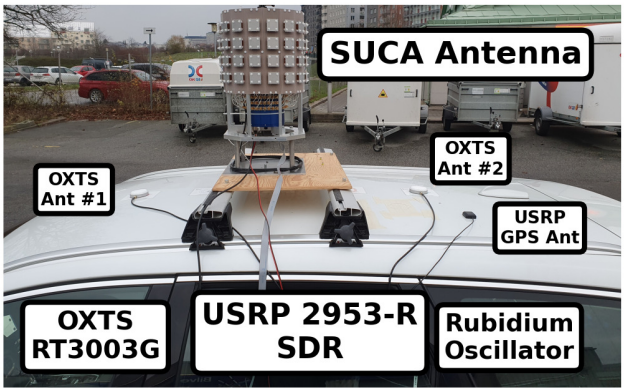

Fig. 8: System components for measurements. The SDR controls the antenna switching and has the same external time synchronization as the OXTS 3003G Ground Truth System.

To verify the clustering concept on measured data, a passenger vehicle was equipped with a massive 128-port Stacked Uniform Circular Array (SUCA), connected to and controlled by a Software-Defined Radio (SDR), which was programmed to receive Cell-Specific Reference Symbols (CRS) from commercial LTE base stations operating at 2.66 GHz. For a detailed description of the test system and signal processing, readers are referred to [14]. Channel estimates for MPCs were generated in post-processing on a snapshot-by-snapshot basis at 75 ms intervals by employing the SAGE algorithm [15]. Angles-of-arrival, delays and signal power are estimated, but CRS are transmitted on only one antenna port at a time, precluding estimation of angles of departure.

The vehicle was driven through an urban canyon environment, with four to five story buildings, as shown in Fig. 9, initially with LOS and then losing it for the remainder of the test drive. The route is split into two sections for illustration and analysis. The transition from LOS to non-LOS occurs during Segment A (which has a duration of approximately 215 meters), and then four laps, two in each direction, define Segment B (approximately 370 meters per lap), to examine repeatability of the proposed clustering algorithm. The measurements were made around mid-day, and the presence of other vehicles including city buses entailed variable start and stop locations. The Northern and Southern sections of Section B are one-way streets which also necessitated different speeds and start/stop intervals from lap to lap.

IV. Results

The clusters from Section A of the drive route are shown in projection space and overlaid on a map in Fig. 10. MPC angles of arrival are clearly governed by the geometry of the

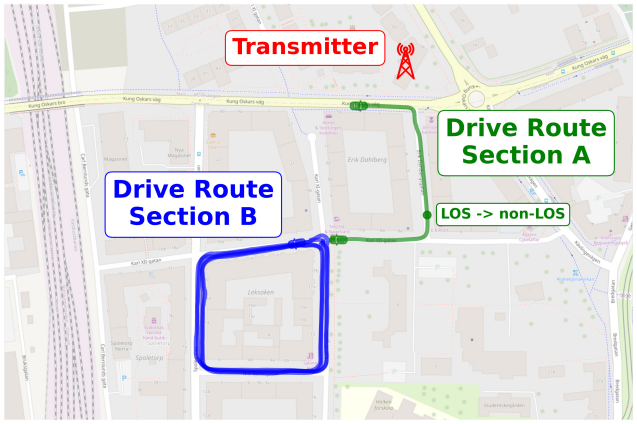

Fig. 9: Drive route in downtown Lund, Sweden (approximate location 55.71°N, 13.19°E). The route is split into Segment A for illustrating MPCs in projection space and Segment B for analyzing repeatability of the proposed clustering algorithm.

surrounding buildings and clustered accordingly. Points to the East intersect a building with segments of wall spaced about 20 meters apart, which are the plausible source of the reflections giving rise to these clusters. Multiple projected points seem to correspond with objects in the vicinity of the transmitter. After the transition to non-LOS, the large buildings farther to the South and East appear to be the dominant source of clustered MPCs. When the vehicle starts to enter the urban canyon at the end of the route, the clusters are large and split into Northern and Southern segments. This indicates close proximity to the cluster ellipsoids in the street canyon.

Statistics regarding the number of snapshots, MPCs, and clusters together with VR durations from the four laps of Section B of the Drive Route are shown in Table I. The four laps have a variable number of 75-ms snapshots because starts, stops and exact locations were governed by other traffic and two laps (1 and 4) were driven counter-clockwise while the

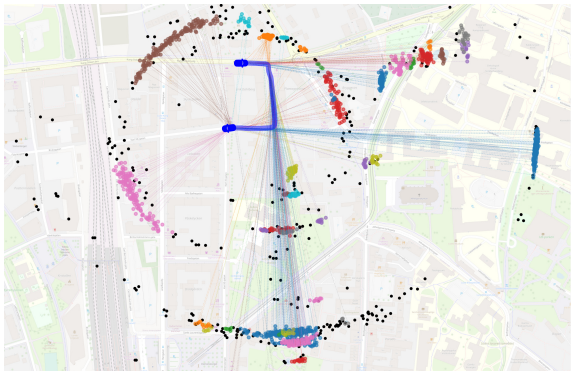

Fig. 10: Clusters in projection space, overlaid on a map. MPCs belonging to the same cluster are shown in the same color (some colors are re-used) and discarded MPCs (noise, for DBSCAN) are illustrated as black with no connecting segments. Not all MPCs are shown to reduce visual clutter.

TABLE I: Clustering Statistics - Section B

Parameter	Lap 1	Lap 2	Lap 3	Lap 4
Number of Snapshots T	5049	5377	5051	4953
Number of MPCs	18602	22917	24587	24293
Number of Clusters P	70	72	61	53
% of MPCs Clustered	66	62	68	66
Median Cluster VR (m)	11.9	12.3	12.9	10.8
Max Cluster VR (m)	62	61	70	62

others (2 and 3) were driven clockwise. A similar percentage of estimated MPCs is clustered in all passes. If it were desirable to increase the percentage of clustered components, the tuning parameter N_{min} could be decreased in order to relax the requirement on the number of proximate MPCs in odometry space necessary for cluster formation, and the parameter ϵ can be increased for more liberal definitions of ϵ-neighborhoods. Ultimately, the percentage of clustered MPCs and the number of clusters are functions not only of the measurement apparatus resolution in time and space, but are also a function of speed and snapshot interval duration. A slowly-moving vehicle, or a faster snapshot interval will result in proportionally more MPCs for potential clustering, because more snapshots will aggregate while moving through each VR. The number of clusters is relatively consistent from lap to lap, as are the median VR lengths. The maximum VR for all laps is associated with a reflecting object to the East, visible for the entire Northern section of the route before rounding the corner. Cumulative distribution functions of VR lengths for each lap are shown in Fig. 11.

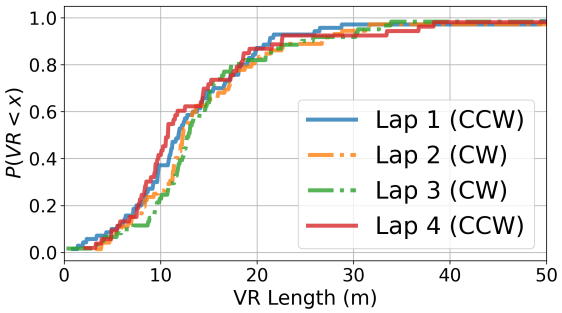

Fig. 11: Cumulative distribution function of VR lengths for the four laps, two clockwise (CW) and two counter-clockwise (CCW).

V. CONCLUSION

The algorithm is shown to produce similar cluster statistics with multiple passes over the same test route (in opposing directions) even in a complicated propagation environment with irregular surfaces, limited signal bandwidth, and in non-LOS conditions with no tuning parameters required other than a distance metric ϵ and a minimum number of adjacent points N_{min} for determining core points, which can be quickly and intuitively analyzed by examining channel estimation results in projection space or odometry space.

Future work could introduce heuristics for cluster combination and classification. Measurements with a system enabling estimation of angles-of-departure would add additional dimensions in which to perform clustering. Additionally, integration of "dense multipath" into the clustering framework could offer additional insight, as well as the integration of Doppler shifts and polarization.

ACKNOWLEDGEMENT

This work was financed in part by the Swedish Innovation Agency VINNOVA through the MIMO-PAD Project (Reference number 2018-05000). Computational resources were provided by the Swedish National Infrastructure for Computing (SNIC) at HPC2N, partially funded by the Swedish Research Council through grant agreement no. 2018-05973. The authors would like to thank Martin Nilsson for his help in setting up the measurement system.

REFERENCES

[1] M. Series, "IMT vision–framework and overall objectives of the future development of IMT for 2020 and beyond," *Recommendation ITU*, vol. 2083, no. 0, 2015.

[2] M. Bennis, M. Debbah, and H. V. Poor, "Ultrareliable and low-latency wireless communication: Tail, risk, and scale," *Proceedings of the IEEE*, vol. 106, no. 10, pp. 1834–1853, 2018.

[3] N. Czink, "The random-cluster model - a stochastic MIMO channel model for broadband wireless communication systems of the 3rd generation and beyond," Ph.D. dissertation, Vienna University of Technology, 12 2007.

[4] S. Jiang, W. Wang *et al.*, "A survey of dense multipath and its impact on wireless systems," *IEEE Open Journal of Antennas and Propagation*, 2022.

[5] K. Haneda, R. Rudd *et al.*, "Radio propagation modeling methods and tools," in *Inclusive Radio Communications for 5G and Beyond*. Elsevier, 2021, pp. 7–48.

[6] H. Tataria, K. Haneda *et al.*, "Standardization of propagation models for terrestrial cellular systems: A historical perspective," *International Journal of Wireless Information Networks*, vol. 28, pp. 20–44, 2021.

[7] M. Ester, H.-P. Kriegel *et al.*, "A density-based algorithm for discovering clusters in large spatial databases with noise," ser. KDD'96. AAAI Press, 1996, p. 226–231.

[8] A. A. Saleh and R. Valenzuela, "A statistical model for indoor multipath propagation," *IEEE Journal on selected areas in communications*, vol. 5, no. 2, pp. 128–137, 1987.

[9] L. Liu, C. Oestges *et al.*, "The COST 2100 MIMO channel model," *IEEE Wireless Communications*, vol. 19, no. 6, pp. 92–99, 2012.

[10] R. He, Q. Li *et al.*, "A kernel-power-density-based algorithm for channel multipath components clustering," *IEEE Transactions on Wireless Communications*, vol. 16, no. 11, pp. 7138–7151, 2017.

[11] Y. Ge, F. Wen *et al.*, "5G SLAM using the clustering and assignment approach with diffuse multipath," *Sensors*, vol. 20, no. 16, p. 4656, 2020.

[12] M. Zhu, G. Eriksson, and F. Tufvesson, "The COST 2100 channel model: Parameterization and validation based on outdoor MIMO measurements at 300 MHz," *IEEE transactions on wireless communications*, vol. 12, no. 2, pp. 888–897, 2013.

[13] K. Khan, S. U. Rehman *et al.*, "DBSCAN: Past, present and future," in *The fifth international conference on the applications of digital information and web technologies (ICADIWT 2014)*. IEEE, 2014, pp. 232–238.

[14] J. Chen, R. Whiton *et al.*, "High-resolution channel sounding and parameter estimation in multi-site cellular networks," in *2023 Joint European Conference on Networks and Communications & 6G Summit (EuCNC/6G Summit)*. IEEE, 2023, pp. 1–6.

[15] B. H. Fleury, M. Tschudin *et al.*, "Channel parameter estimation in mobile radio environments using the SAGE algorithm," *IEEE Journal on selected areas in communications*, vol. 17, no. 3, pp. 434–450, 1999.